Operating Coupled VO-Based Oscillators for Solving Ising Models

Operating Coupled VO_2-Based Oscillators for Solving Ising Models

María J. Avedillo, Manuel Jiménez Través, *Member, IEEE*, Corentin Delacour, Aida Todri-Sanial, Bernabé Linares-Barranco, and Juan Núñez

***Abstract*— Coupled nano-oscillators are attracting increasing interest because of their potential to perform computation efficiently, enabling new applications in computing and information processing. The potential of phase transition devices for such dynamical systems has recently been recognized. This paper investigates the implementation of coupled VO_2-based oscillator networks to solve combinatorial optimization problems. The target problem is mapped to an Ising model, which is solved by the synchronization dynamics of the system. Different factors that impact the probability of the system reaching the ground state of the Ising Hamiltonian and, therefore, the optimum solution to the corresponding optimization problem, are analyzed. The simulation-based analysis has led to the proposal of a novel Second-Harmonic Injection Locking (SHIL) schedule. Its main feature is that SHIL signal amplitude is repeatedly smoothly increased and decreased. Reducing SHIL strength is the mechanism that enables escaping from local minimum energy states. Our experiments show better results in terms of success probability than previously reported approaches. An experimental Oscillatory Ising Machine (OIM) has been built to validate our proposal.**

***Index Terms*— Phase transition devices, VO_2, coupled oscillators, oscillation based computing, phase locking, ising machine, combinatorial optimization.**

I. Introduction

CURRENT computing platforms demand fast and energy-efficient solutions to computationally hard and data-intensive problems. Solutions to these challenges are currently being investigated from many different perspectives, including techniques at the physical, circuit, architectural, or system level. More breakthrough approaches to provide medium-term solutions, explore different devices to replace or complement the MOS transistor, as well as alternative computing paradigms.

An active research area that merges both approaches is that of oscillator-based computing (OBC) and its synchronization phenomena [1], [2], [3], [4]. The idea is to take advantage of the rich dynamics of coupled oscillator systems and implement them with compact and very low-energy oscillators enabled by emerging technologies. In particular, Phase Shift Key (PSK) OBC uses oscillators of ideally identical frequency, and the processing corresponds to obtaining a phase pattern for the oscillation phases of the coupled oscillators.

Combinatorial optimization problems (COPs) are hard computational problems encountered in many areas of activity with great economic impact, such as finance, manufacturing, mobility, logistics, or cryptography [5]. This means that the development of hardware platforms that allow them to be solved more efficiently than using conventional computers is of great interest. It is well known that many relevant COPs can be mapped to an Ising model [6], a mathematical model of the statistical mechanics to study ferromagnetism. So, there are many efforts to develop efficient Ising solvers or Ising machines. There are already available pure CMOS digital solutions [7], but also quantum-based ones [8], which are referred as annealers. Research using alternative physics-based computing paradigms to keep the advantages of the quantum approach, but without exhibiting its disadvantages such as operating temperature, is being conducted.

In particular, recently, PSK OBC Ising machines with coupled oscillators that exploit their dynamics of evolution towards a minimal energy state have been explored from different points of view. Implementations using different technologies have been proposed and experimentally validated. In particular, an experimental implementation of an Ising solver using coupled phase-transition nano-oscillators with VO_2 devices has been reported [9]. Experimentally calibrated numerical simulations show they exhibit high energy efficiency and potential for several orders of magnitude improvement over CPU, GPU, quantum and photonic approaches [10].

VO_2 devices have also been applied to realize associative memory functionality. The authors have developed different architectures for this application [11], [12], [13], [14], [15], [16]. Based on this experience, we address now the implementation of Ising machines. We claim that both applications are somehow two faces of the same coin and that each one

Manuscript received 3 May 2023; revised 2 August 2023 and 15 September 2023; accepted 24 October 2023. Date of publication 31 October 2023; date of current version 29 December 2023. This work was supported in part by the NeurONN Project (Horizon 2020) under Grant 871501; in part by Fondo Europeo de Desarrollo Regional (FEDER); and in part by Consejería de Transformación Económica, Industria, Conocimiento y Universidades de la Junta de Andalucía, dentro del Programa Operativo FEDER 2014-2020, under Project US-1380876. This article was recommended by Guest Editor C. Lammie. *(Corresponding author: Juan Núñez.)*

María J. Avedillo, Manuel Jiménez Través, Bernabé Linares-Barranco, and Juan Núñez are with the Instituto de Microelectrónica de Sevilla, IMSE-CNM, (CSIC/Universidad de Sevilla), 41092 Sevilla, Spain (e-mail: jnunez@imse-cnm.csic.es).

Corentin Delacour is with LIRMM, University of Montpellier, 56227 Montpellier, France.

Aida Todri-Sanial is with LIRMM, University of Montpellier, 56227 Montpellier, France, and also with the Electrical Engineering Department, Eindhoven University of Technology, 5612 AZ Eindhoven, The Netherlands.

Color versions of one or more figures in this article are available at https://doi.org/10.1109/JETCAS.2023.3328887.

Digital Object Identifier 10.1109/JETCAS.2023.3328887

requires to be operated differently. Implementation features that are drawbacks for one of them can be beneficial for the other. This analysis leads to propose an operating protocol for oscillation-based Ising machines, supported both by simulation and hardware experiments. The suitable operation of Ising machines is comprehensively addressed in [17], where an in-depth analysis of the performance of a network of coupled stochastic injection-locked VO_2 oscillators is presented in terms of its Lyapunov energy and its continuous-time dynamics and how the latter can be harnessed to perform classical annealing. On this basis, we further investigate other factors that can also affect Ising solver performance. Unlike the mentioned work, the simulation results correspond to transient electrical simulations using a model for VO_2 devices which incorporates stochasticity, instead of oscillator models in the phase domain that introduce phase noise. Moreover, experimental validation is also carried out. Our simulation and experimental results solving Max-Cut optimization problems contribute to a deeper understanding of how to operate a network of coupled oscillators as an Ising machine.

The rest of the paper is organized as follows. Section II introduces VO_2 oscillators, the applications of coupled oscillator systems, and the Ising machine concept. Section III is devoted to the suitable operation for the Ising machine application. Extensive simulations are described to introduce the different factors which impact its behavior and introduce a proposal for operating it. Section IV describes experiments carried out with a hardware implementation of an oscillator-based Ising machine to support our proposal. Finally, Section VI is devoted to the conclusions.

II. Background

A. VO2 Oscillators

VO_2 undergoes metal-insulator transitions under given electrical stimuli. That is, abrupt switching occurs from/to a high resistivity state (insulating phase) to/from a low resistivity state (metallic phase). Without electrical stimuli, VO_2 tends to stabilize in the insulating phase. When the applied voltage increases and the current density flowing through it reaches J_{C-IMT}, an insulator-to-metal transition (IMT) occurs. Once in the metallic state, when the voltage decreases and the current density drops below J_{C-MIT}, metal-to-insulator transition (MIT) takes place. Fig 1a shows the I-V characteristic of a generic VO_2 device. V_{IMT} (V_{MIT}) is the voltage at which the insulator-to-metal transition, (IMT) (metal-to-insulator transition, MIT) occurs. R_{INS} (R_{MET}) is the resistance in the insulating (metallic) state. Since MIT and IMT transitions are abrupt but not instantaneous, transition times (TT_{IMT}, TT_{MIT}) are also considered.

For simulations, the behavioral Verilog-A model of the VO_2 device reported in [18] is selected. In this work, we use the VO_2 device with the electrical parameters shown in TABLE I [19].

Fig 1b shows a VO_2-based oscillator [18], [20]. It consists of a VO_2 device through which a capacitance C is charged, which is discharged through a resistance R. Fig 1c depicts waveforms for the oscillator output. The state of the VO_2 is also shown

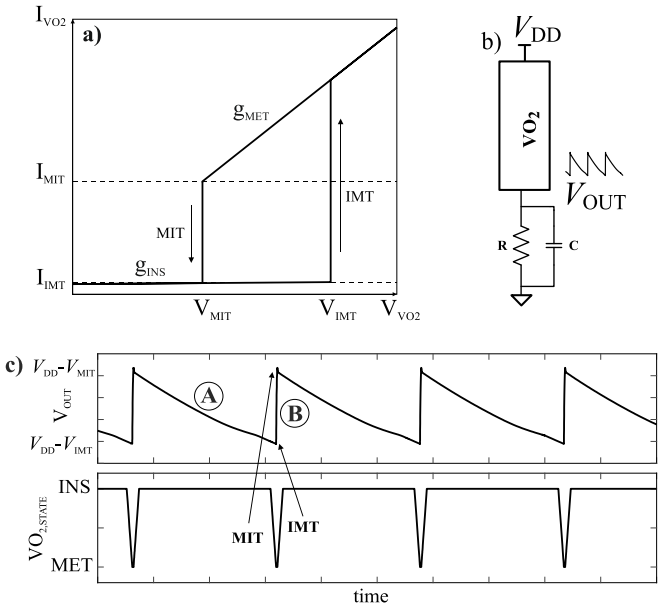

Fig. 1. (a) Generic I-V curve of a VO_2 device. VO_2 oscillator (b) circuit topology, (c) operation waveforms in which points corresponding to insulator-to-metal and metal-to-insulator transitions have been marked with arrows.

TABLE I
VO_2 ELECTRICAL PARAMETERS

PARAMETER	VALUE
V_{IMT}	1.99V
V_{MIT}	0.99V
R_{MET}	0.99KΩ
R_{INS}	100.2KΩ
TT	30ns

to better illustrate the circuit behavior. $VO_{2,STATE}$ = 'INS' means the device is in the insulating state. $VO_{2,STATE}$ = 'MET' corresponds to the device in the metallic state. Assuming that the VO_2 is in an insulating state (marked with "A" in Fig 1c), the oscillator output is discharged through the resistor. This increases the voltage drop across the VO_2 ($V_{DD} - V_{OUT}$) and so the current through it increases. Once enough current density circulates (J_{C-IMT}), it switches to the metallic state (marked with "B" in Fig 1c). Equivalently, using the electrical model, switching to the metallic state occurs once the VO_2 voltage reaches V_{IMT}. The capacitor is then charged through the VO_2. This charging is very fast because of the low R_{MET} value. The voltage seen by the VO_2 decreases until it reaches V_{MIT} and the transition from metal to insulator state occurs.

B. Coupled Oscillator Networks

Oscillator Based Computation (OBC) relies on the dynamics of coupled oscillator systems. It has received considerable interest and has become an active research area due to the emergence of devices, operating on the basis of very different physical phenomena, with the ability to implement very compact oscillators and with very low power consumption. Instead of using voltage levels as logic levels, the phase differences between an oscillator signal and a reference signal are used.

Recent works have shown that almost all types of nonlinear self-sustaining oscillators are suitable to implement systems with the inherent convergence property towards a minimal energy state. This can be applied to implement different functionalities by suitably configuring the couplings so that the minimal energy states are the solutions to the target problem. In [2] and [21], the graph coloring problem (GC) is solved from the steady state of a network of oscillators, which represent the nodes, and where the branches of the corresponding graph are mapped in interconnections that push to separate the phases of the adjacent oscillators. Associative memory applications (AM) derive coupling strengths so that the patterns to be stored correspond to minimal energy states of the network. Similarly, combinatorial optimization problems can be solved by coupled oscillator systems embedding the target solution into the ground state of the system. For this, the Ising model concept described in the next subsection is used.

C. Ising Machine

It is well-known that a wide variety of NP optimization problems can be formulated as an Ising model. An Ising model is a mathematical model used in statistical mechanics to study ferromagnetism. It is composed of N binary spins, $\sigma_i \in \{\pm 1\}$, and interactions between pairs of spins, Jij denotes the interaction between spin $i$and spin j.The Ising Hamiltonian is a function of the spin configuration of the system, defined as:

$$H(\sigma) = -\sum\nolimits_{i<j} J_{i,j}\sigma_i\sigma_j (1 \le i, j \le N) \tag{1}$$

Solving an Ising model corresponds to determining the spin configuration which minimizes H(ground state).Solving an Ising model is itself an NP hard problem [6].

A special type of computer, called an Ising machine (IM) or Ising solver, solves Ising models. Thus, it has been put forward as an efficient way of performing optimization. An IM solves a class of optimization problems by mapping them to the Ising Hamiltonian of a spin glass system and finding its ground state solution.

In this paper, the unweighted Max-Cut problem, a well know optimization problem which can be mapped to an Ising model, has been selected for our experiments. A maximum cut of a graph is a partition of the vertices of the graph into two complementary sets such that the number of edges between them is the largest possible. The problem of finding a maximum cut in a graph is known as the Max-Cut problem. Formally, it can be formulated as follows. Given an unweighted graph $G = (V, E)$, where V are the vertices and E are the edges between them, the solution of the Max-Cut problem provides a disjoint partition $V_1 \cup V_2 = V$ such that the cardinal of set $E' = \{(u, v), (u, v) \in E, u \in V_1, v \in V_2\}$ is maximized.

Assuming:

$$x_i = \begin{cases} 1 \; if \; i \in V_2 \\ 0 \; if \; i \in V_1 \end{cases} \tag{2}$$

the value of the cut can be written as:

$$C = \sum_{i<j} w_{i,j} \frac{(1 - x_i x_j)}{2} = \frac{1}{2}\sum\nolimits_{i<j} w_{i,j} - \frac{1}{2}\sum\nolimits_{i<j} w_{i,j} x_i x_j \tag{3}$$

where $w_{i,j} = 1$ if $(I, j) \in E$ and 0 otherwise. Thus, the relationship with the Ising model is evident. C can be written in terms of the Hamiltonian in (1):

$$C = \frac{1}{2}\sum\nolimits_{i<j} w_{i,j} - \frac{1}{2}H(x) \tag{4}$$

with $J_{i,j} = -w_{i,j} = -1$. Note that the first term is constant and that by minimizing H, the value of cut, C, is maximized.

In [22], IMs are classified into three main categories according to their operating principle: classical annealing, quantum annealing, and dynamical system evolution, although different operating principles can be combined. Examples of digital dedicated annealers are the Fujitsu digital annealer [7], [23], the Toshiba bifurcation machine [24] or the FPGA-based solution reported in [25]. In the analog domain, it has been proposed to exploit the intrinsic randomness of nanodevices to avoid the area and energy cost associated to the pseudo-random number generators required in their digital counterparts, also improving the quality of randomness. For example, using magnetic tunnel junctions [26], [27]. In [8] a quantum annealer built by D-Wave Systems is reported. However, it suffers from various problems. These included the need to operate at a temperature close to absolute zero as well as the difficulty of scaling up the machine size, a consequence of its use of quantum techniques. The third type of IM is based on the evolution of a dynamical system in which the state of the system is naturally driven towards the lowest energy state of the Ising model. In particular, coupled oscillators exhibit such behavior and several oscillation-based IMs (OIMs) have been proposed using very different types of oscillators, including optical parametric oscillators, [28], [29], [30], electronic conventional ones, such as discrete LC oscillators [31], [32], [33], ring oscillators [34], [35], differential oscillators [36] or Schmitt Trigger oscillators [17], as well as other built based on non-conventional devices like phase transition materials [9], [10], Ferroelectric transistors [37] or spin torque devices [38].

III. Operating Coupled Oscillator Systems

Each of the three applications of coupled oscillator networks enumerated in Section II-B (GC, AM, IM) requires being operated differently. Let us illustrate this with the simple four-oscillator system in Fig.2.

A. Graph Coloring

The graph coloring problem assigns a colour to each vertex of a graph such that any two adjacent vertices have different colors while minimizing the number of colors.

The network in Fig.2 can solve the graph coloring problem corresponding to the graph in Fig.3a in which each node is adjacent to every other. Thus, four colors are necessary to color it. Fig.3b depicts the simulated waveforms. Note that after several oscillation cycles, there are four stable phases 90° apart.

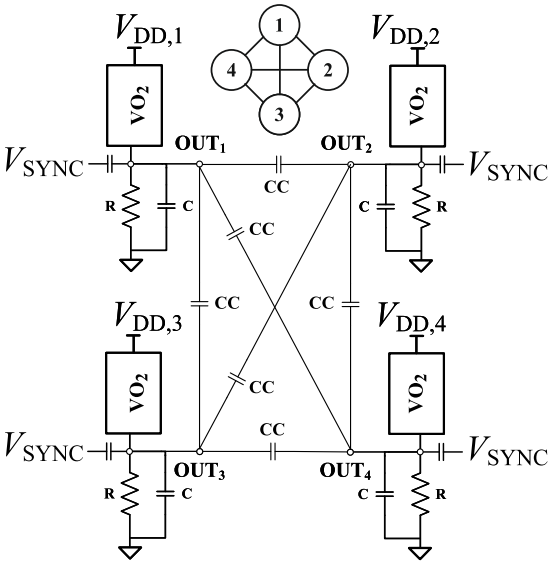

Fig. 2. Schematic of a coupled oscillator system.

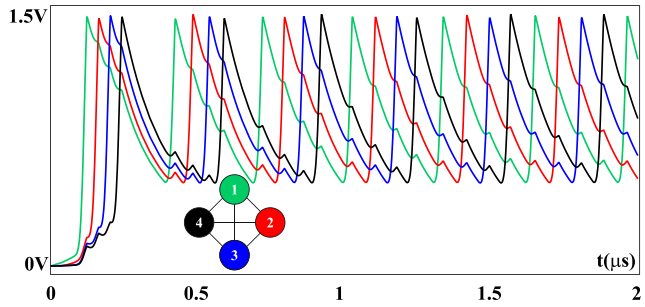

Fig. 3. Circuit in Fig.2 solving the graph colouring problem.

B. Associative Memory (AM)

A coupled oscillator network resembles a Hopfield Neural Network (HNN). An HNN is a recurrent neural network defined by a symmetric weight matrix W, and an update rule. W_{ij} denotes the weight associated with the connection between neuron i and j. Furthermore, in its discrete and synchronous version, each neuron state, s_i, operates with bipolar values $(1, -1)$ and is updated simultaneously as:

$$s_i = sign(\sum_j w_{ij} s_j) \tag{5}$$

The stored patterns are those state of the system which are fixed points of (2).

Under this model, the network in Fig.2 has the weight matrix shown in Fig 4a and it is storing any pattern with exactly two zeros and two ones, as depicted in Fig 4b. Using the HNN as associative memory requires applying a test pattern, which if it is not a stored one, should evolve towards the closest stored one. It is said to be retrieved or inferred.

Therefore, for this application, only two phases should be possible for the oscillators to represent '1' and "−1". This is different from the requirements of the graph coloring application. Additionally, it is critical to the initial state of the coupled oscillator network.

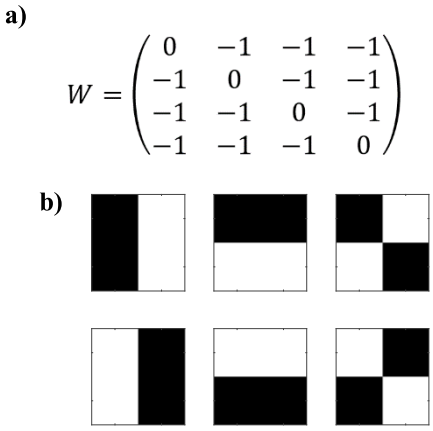

Fig. 4. (a) HNN weight matrix associated with the system in Fig.2. (b) Patterns stored in the HNN.

The first requirement is achieved through Second-Harmonic Injection Locking (SHIL) [39]. When a suitable synchronization signal (V_{SYNC}) of frequency f_{SYNC} is injected to an oscillator of the natural frequency close enough to f_{SYNC}/N, SHIL occurs and the oscillator adopts a frequency equal to f_{SYNC}/N and becomes phase synchronized within one of N possible phases that are $(360/N)°$ apart. $N = 2$ is used to work with two phases.

In these oscillators, the initialization is carried out through the pulsed bias signal, which rises from the ground to a constant value (V_{DD}) after a certain delay. This delay is closely linked to the oscillation period, so that for two coupled oscillators, they could be initialized in phase or out-of-phase simply by making the difference between the switching times of their polarization zero and half a period respectively [19].

The operation of a fully connected 4-node oscillator network (Fig.2) operating as AM is illustrated in Fig.5. For this purpose, the grayscale input pattern shown in Fig.5a is applied, with which an output pattern as shown in the same figure (and also in Fig 4b) should be retrieved. The waveforms corresponding to this example are depicted in Fig.5b. Note how the outputs switch at different instants, corresponding to the delayed initialization according to the applied input pattern. As expected, outputs 1 and 2 are in one phase, while outputs 3 and 4 are 180 degrees apart.

C. Ising Machine (IM)

The network in Fig.2 can also be described as an Ising machine to solve the Max-Cut optimization problem for the graph in Fig.3a. The network is operated and the final distribution of the oscillator phases defines the two partitions. Clearly, SHIL is also a requirement to discretize into two possible phases.

Clearly, a partition with any two vertices in each one is a Max-Cut of the graph under analysis. All those corresponding network states have the same Hamiltonian energy, and this is the minimum among all possible states.

Fig.6 depicts waveforms for the system in Fig.2 which correspond to the Ising solver for the Max-Cut of the complete graph in Fig.3a. The four oscillators are initialized in phase and the system evolves towards an optimal solution (4 cuts)

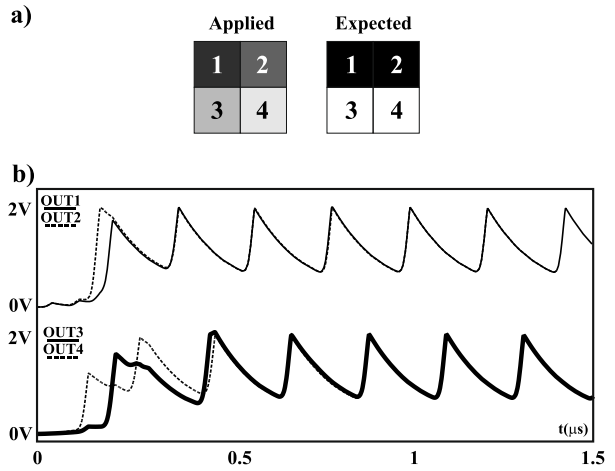

Fig. 5. Operation of a fully connected 4-node HNN for AM applications. (a) Applied and expected patterns to the HNN. (b) Output waveforms.

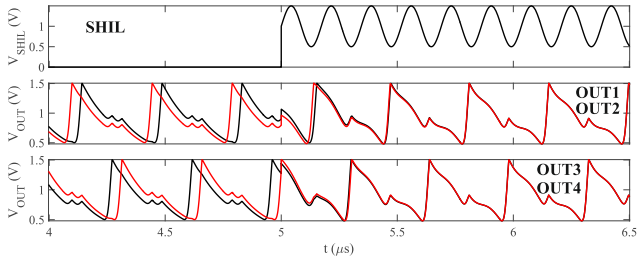

Fig. 6. Circuit in Fig.2 solving the Max-Cut optimization problem.

in which two oscillators exhibit one phase and the other two the complementary one. It can also be observed that after the application of SHIL (5μs), there are only two possible phases. Note the difference with the waveforms in Fig.3, corresponding to the simulation of the same circuit but without applying SHIL.

These simple examples have been useful to explain how depending on the operation conditions of the same coupled oscillator system, solutions to different problems can be obtained. Graph colouring does not require SHIL while the other two do. However, we claim that operation as associative memory and as Ising machine should be completely different. Moreover, what can benefit one application could be dramatic for the other.

On the one hand, thinking in terms of the system energy landscape, configured by the couplings, can help to understand this statement. The system dynamics naturally evolves to states with less energy, but the system can be trapped at a local minimum. From the point of view of the optimization problems, this impedes obtaining the optimum solution. Unlike this, this local minimal can correspond to the store pattern closest to the applied test pattern. In the first case, being able to escape from it is positive, as it could improve the quality of the solution, but it is negative in the second one since a wrong pattern could be retrieved, reducing accuracy. The role of SHIL and stochasticity in escaping from local minima is being investigated.

Additionally, considering the probabilistic nature requirement of OIMs can also be useful in realizing the differences

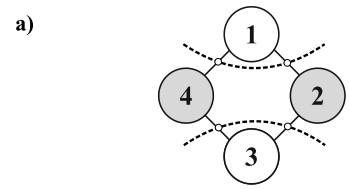

b)

(σ3,σ4) \ (σ1,σ2)	(1,1)	(1,-1)	(-1,-1)	(-1,1)
(1,1)	1	0	0	0
(1,-1)	0	-1	0	0
(-1,-1)	0	0	1	0
(-1,1)	0	0	0	-1

Fig. 7. Fully interconnected 4-node Max-Cut problem. (a) Optimal solution (4 cuts). (b) Energy landscape.

between both applications since a nondeterministic behavior is not compatible with the AM application. In this respect, noise or cycle-to-cycle variability is very well welcomed for OIMs, but should be kept under control for associative memory operation. Because of this probabilistic nature, there is no guarantee that the optimum solution (or ground state) is reached. The probability of reaching it is called success probability and is widely used as a figure of merit in the performance of IMs. Thus, the performance of many trials is often reported in the literature as a mechanism to increase the quality of the solutions. Note that the probability of success can be closely related to the problem to be solved. It seems reasonable to assume that, for problems with a high number of vertices, the probability of reaching a local minimum is smaller than in a simpler one [10].

We have designed a set of experiments to gain insight into the factors pointed out in previous paragraphs and their relationships to derive how to operate coupled oscillators to achieve good performance as IMs.

IV. Operating Coupled Oscillator-Based IMs

A. Analysis of Factors

To explore the role of the SHIL signal, noise, initial phase relationship, and coupling strength in the operation of coupled oscillators as IMs, the behavior of a solver of the Max-Cut problem in Fig 7a is further investigated. Its energy landscape is depicted in Fig 7b. The Hamiltonian energy for the sixteen spin configurations is shown using a Karnaugh map as a representation. That is, spin configurations associated with adjacent cells differ in a single spin. There are two global minimum energy configurations which have been marked. Any of them is a solution to the corresponding Max-Cut problem. As expected, these global minimum energy configurations have spins 1 and 3 at the same value, and spins 2 and 4 take the opposite value. It corresponds to the optimum Max-Cut (cut value equal to 4) shown in Fig 7a. To be successful in solving the associated optimization problem, the oscillator system should evolve to a one of those spin configurations.

SHIL signal strength, noise and coupling strength are closely related. In our simulation experiments, we keep the

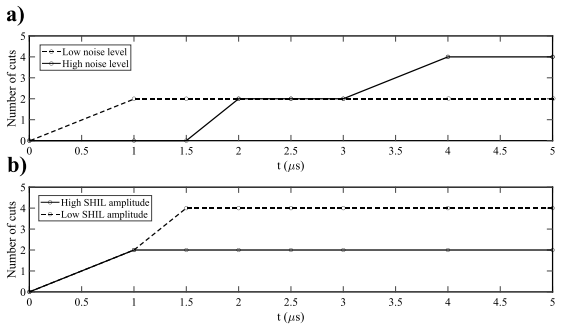

Fig. 8. Evolution of the number of cuts with time for two different noise levels (a) and two different SHIL amplitudes (b).

coupling strength fixed and illustrate the impact and relationship of the other two.

A key component of hardware IMs that can be fundamental in efficiently solving COPs is the internal noise of the circuit, which helps escape from suboptimal solutions (local energy minimum). In fact, in digital IMs, random number generators are used for this. Moreover, different authors have stated the critical role of inherent stochasticity in the implementation of IMs, which is identified with a probabilistic exploration [10], [34]. Because of this, they report that many trials are conducted so that the chance of obtaining the optimum solution increases.

It is well-known and has been reported in the literature that actual VO_2 devices exhibit variability in the state transition voltages. In [40] it is reported that V_{IMT} exhibits variability more than seven times larger than for V_{MIT}. It is also reported that it varies stochastically for all cycles without a reduction in the mean or range and can be approximated by a normal distribution. Additionally, the impact of the insulating-to-metal variability in the performance of coupled oscillator systems is much greater than the one associated with the reverse phase transition [12]. Thus, a cycle-to-cycle variability of its insulating to metal voltage (V_{IMT}) has been included in the VO_2 model described in Section II-A. A normal distribution is associated with it. That is, V_{IMT} changes in time following a normal distribution around its nominal value, with a given standard deviation denoted σ_{NOISE} or noise level. It translates in cycle-to-cycle variations in the oscillation period (jitter). The chosen name refers to the fact that it, not only allows us to model the experimental variability observed in said parameter, but also allows to capture the effect of other noise sources that manifest as jitter in the oscillation period. Note that there is also mathematical noise associated with the integration algorithms and their tolerances.

Fig 8a shows simulation results for the cut value associated with the evolution of the 4-oscillator system representing the graph of Fig 7a with two different noise levels. Identical initial state and synchronization signals have been used in both simulations. It can be observed that the system with a very small noise level becomes trapped in a local minimum with a cut-value equal to 2, not a maximum. The system with more noise can reach the global optimum (minimum energy spin configuration).

Fig 8b depicts the result of simulations with a very small noise level and two different amplitudes for the

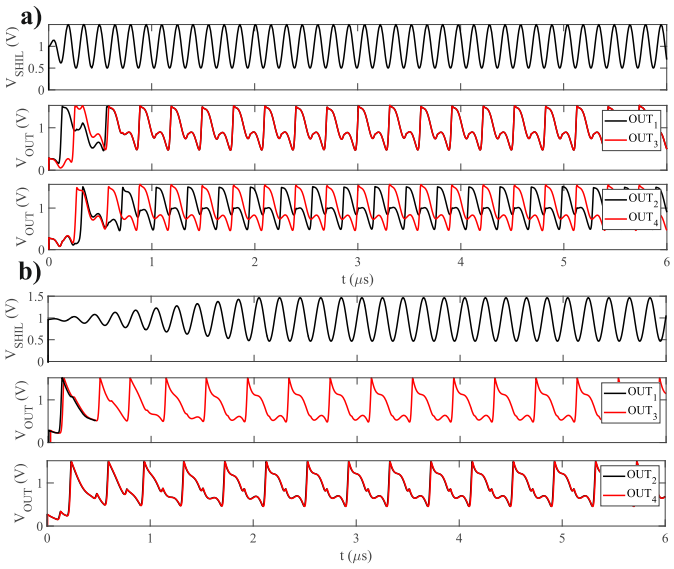

Fig. 9. Waveforms for two SHIL schedules, (a) constant amplitude and (b) increasing amplitude.

synchronization signal. This experiment shows how SHIL counteracts noise. Reducing the amplitude of the synchronization signal allows escaping from the local minimum. That is, as already mentioned, there is a relationship between the different factors involved in the dynamic evolution of the coupled oscillator system.

Another point to take into account is the SHIL signal scheduling. Different scheduling's have been proposed in the literature. In particular, an improvement in the success probability of reaching the optimum solution has been reported by linearly increasing SHIL amplitude compared to a constant SHIL [41] This has been compared to a thermal annealing process in which the reduction of the temperature is associated with the reduction of the stochastic noise in the system as a consequence of the increase in the amplitude of SHIL signal.

Fig 9 illustrates the potential of using a SHIL with smoothly increases its amplitude and its impact on the system. It can be observed that the application of the constant amplitude SHIL signal freezes the system in a non-optimum phase relationship with three oscillators in one phase (cut value equal to 2). This is in agreement with [29] in which it is stated that the freeze-out effects associated with the discretization of the oscillator phases are a limitation for the synchronization dynamics.

In [42], we showed results that the success probability can also be increased by delaying the application of the synchronization signal. In both cases, we are giving time for the system to evolve towards a minimal energy state before forcing a binary discretization of the oscillator phases, which occurs for an enough large SHIL amplitude. Contrary, if a strong enough synchronization signal is applied from the very beginning or too early, the system gets stuck in a stable state in the neighborhood of the initial one which, in general, can be suboptimal. That is a local minimum.

Finally, the initial state of the system (phase relationships) also impacts its dynamics. However, this has not been discussed to the best of our knowledge in the literature. Even if

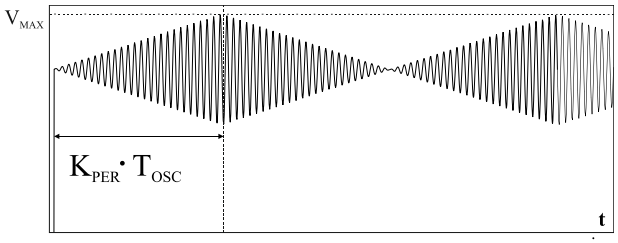

Fig. 10. The proposed SHIL schedule (SHIL3) and the parameters that describe its configuration.

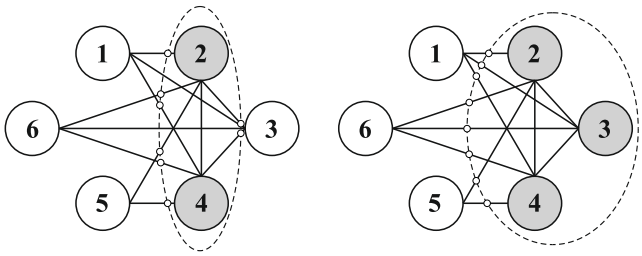

Fig. 11. 6-node Max-Cut problem with two optimum solutions with 8 cuts.

stochasticity is not considered, starting in different initial states can also be advantageous for improving the success probability of optimally solving the associated COP problem.

B. Ising Machine Operation Protocol

On the basis of the analysis of the experiments carried out, we propose the following OIM operating protocol.

- SHIL scheduling according to Fig 10. The V_{MAX} parameter is the signal amplitude, and K_{PER} controls the linear increment/decrement of its amplitude speed. It is measured in cycles of period, T_{OSC}. The amplitude rises from 0 to V_{MAX} in K_{PER} cycles. The repetitive scheme of sweeping SHIL amplitude allows further exploration of the associated energy landscape of the Ising model, such as the use of many trials reported in the literature, and enables an important escape mechanism from local minimum solutions when SHIL strength is reduced.
- The solution is selected on multiple readings and the selection of the best one. This aims to counteract the possibility of escaping a global minimum or worsening the quality of the solution. This could occur because of excessive noise in the system or as a consequence of SHIL strength reduction. Readings must be carried out with enough SHIL signal strength so that phases are binarized and so that the reading process is simplified. Readings are carried out around the points at which the SHIL signal reaches its maximum amplitude. Thus, how many readings take place depends on how long the OIM is operated (T_{COMP}) and K_{PER}.

To evaluate the proposed operation protocol, a second Max-Cut instance, depicted in Fig 11 has been used in the simulation experiments. Note that it exhibits critical difference with respect to the analyzed in the previous subsection (graph in Fig 7). The associated oscillator system presents phase contention. This means that it is not possible to fulfil all phase constraints imposed by the capacitors that connect pairs of oscillators in the associated IM. In addition, it is a non-balanced graph in the sense that nodes exhibit a different number of connections."

The IM associated with the graph in Fig 11 has been evaluated with three different SHIL schedules illustrated in Fig 12: an already introduced increasing amplitude SHIL signal (SHIL1), a SHIL signal periodically switching between two different amplitudes (SHIL2) [43] and the proposed one (SHIL3). The multiple reading approach has been used in all the cases. For each of them, 20 Monte Carlo (MC) runs have been performed for each of the 64 possible initial binary phase combinations. MC analysis is used because of the random distribution included in the VO_2 model. This experiment was carried out for three different values (no noise, 1mV and 10mV). Three T_{COMP} values were analyzed. T_{COMP1} corresponds to 1.5 periods of the SHIL3 signal (2 readings), T_{COMP2} corresponds to 9.5 periods and 10 readings, and T_{COMP3} to 17.5 periods and 18 readings. For selected V_{MAX} and K_{PER}, T_{COMP1} is 12μs. $V_{MAX} = 0.4$V has been chosen so that it is strong enough to produce the desired discretization of the phases and its amplitude is similar to that of the oscillators themselves. $K_{PER} = 20$ has been selected.

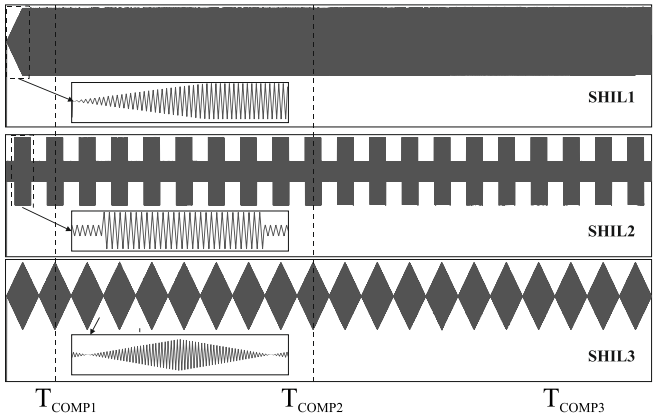

Fig. 12. SHIL schedules used for the evaluation of the OIM.

TABLE II shows the number of initial system states from which an optimum solution is obtained for different computation times. That is, at least one of their associated 20 MC simulations obtained an optimum solution. Note that a single simulation is carried out when no noise is modeled. It is clear that noise is beneficial in increasing the number of successful initial states, although this figure of merit alone does not completely support the above statement, but the improvement observed (especially for the SHIL1 and T_{COMP1}) between 1mV and 10mV of noise also suggests this. It can also be seen that the number of SHIL1 results is much worse than the other two for the shortest computation time. This can be explained since the capability of exploring the energy landscape and so escaping from a local minimum reduces once a strong enough SHIL is applied. Both SHIL2 and SHIL3 benefit from the reduction of the SHIL strength. When the computation time is increased, the chance of escaping due to noise is increased, and so the number of successful initial states for the SHIL1 experiment also increases significantly.

TABLE II
NUMBER OF INITIAL STATES FROM WHICH AN OPTIMUM SOLUTION IS OBTAINED WITH SHIL1, SHIL2, AND SHIL3, RESPECTIVELY

σ_{NOISE}	T_{COMP1}	T_{COMP2}	T_{COMP3}
0mV (no noise)	9, 18, 26	18, 16, 48	21, 49, 58
1mV	31, 61, 64	58, 64, 64	62, 64, 64
10mV	41, 62, 64	55, 64, 64	62, 64, 64

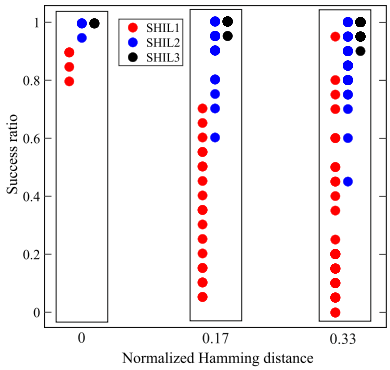

Fig. 13. Success ratio versus Hamming distance between the initial state and the optimum solution for the three SHIL schedules. Simulation parameters: $V_{MAX} = 0.4$V, $\sigma_{NOISE} = 1$mV, T_{COMP3}.

Also, it can be observed that the noise level has little impact but for the SHIL1 and the shortest computation time. This agrees with our above explanation. The higher the noise level increases the probability of escaping from local minima.

Much more insight into system performance can be obtained if the fraction of MC runs achieving the optimum solution is also analyzed. It can be considered as the success probability. A value of 1 for this figure of merit means that the 20 runs produce an optimum solution.

Fig 13 shows such a fraction for each of the 64 initial states versus its normalized Hamming distance to the closest optimum solution. A Hamming distance equal to 0 means that the initial state is an optimum solution to the associated optimization problem. The differences are notorious among the three SHIL schedules. On the one hand, a fraction of successful runs is significantly higher for the proposed SHIL (black points are over 0.8 for all the initial states) than for the other two. The worst results are obtained with SHIL1. The second interesting aspect to be pointed out is that the results are almost independent of the initial state (the 64 points have very little dispersion) for the proposed SHIL while this is not so for the other SHILs, especially for SHIL1. In fact, very few black points appear since many of them occupy the same position. This reduced dependence is also a consequence of reducing the SHIL strength during the operation, allowing a better exploration of the solution space.

It is also interesting to analyze the fraction of successful runs for different computation times. In this analysis, the average and standard deviation over the 64 initial states have been used. A value of 1 for the average means of 1280 (64×20) runs produced an optimum result. Fig 14 depicts the average of the success rate including bars for the standard

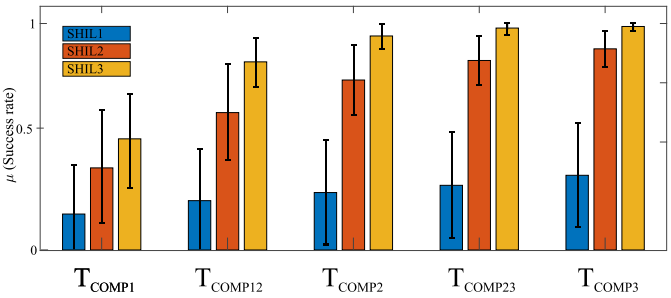

Fig. 14. Average and standard deviation of the success rate for the three SHIL schemes evaluated at five different computation times.

deviation. Note that there are two additional computation times with respect to previous experiments (T_{COMP12} and T_{COMP23}). The limitations of SHIL1 are also evident from this figure. Both SHIL2 and SHIL3 achieved better results in T_{COMP1} than SHIL1 in T_{COMP3}, although T_{COMP1} is around ten times shorter than T_{COMP3}. The smaller standard deviation exhibited by SHIL3 also indicates that the initial state is less relevant for SHIL3, as already pointed out when describing Fig 13.

In [10], the Max-Cut problem depicted in Fig.15a was experimentally solved using VO_2 oscillators and the SHIL schedule identified in this paper as SHIL1. They report a Max-Cut value equal to 10 with a 96% success rate with K_{PER} over 600 oscillation cycles. We have simulated the same graph with SHIL3. Computation time have been fixed to 600 cycles for a fair comparison. In particular, three SHIL3 cycles with $K_{PER} = 100$ have been applied. 20 Monte Carlo simulations for each of 50 different initial states have been carried out. Fig.15b depicts obtained results. Note that Max-Cut values higher than 10 have been obtained. In particular, the optimum solution to the problem (Max-Cut=12) have been obtained in 46.4% of the trials. Moreover, max-cut values equal or greater than 10 have been achieved in 96.1% of all the simulations. The experiment in [10] has been also simulated with our VO_2 models. The optimum Max-Cut value is obtained in 14.8% of the trials.

Additionally, these results indicate that the proposed SHIL scheme could also translate into advantages in terms of energy efficiency. In [10], as already mentioned, analysis results that show the potential of VO_2 based OIMs to drastically increase operations per second and per watt with respect to platforms conventionally used to solve optimization problems are reported. The ability of SHIL3 to achieve higher success rates in shorter computation times could only contribute to increasing this figure of merit with respect to [10] that applied SHIL1.

In summary, this simulation analysis has shown the potential of increasing and decreasing the SHIL amplitude to escape from local minimum energy states in OIMs associated to a six-node Max-Cut problem and the role of noise in this energy landscape exploration. However, experimental validation is mandatory. This work is described in the next section, where, in addition, an exploration of different K_{PER} values to further explore the annealing scheme is included. This was not addressed in the simulation framework due to limitations of computation times. However, we consider it interesting

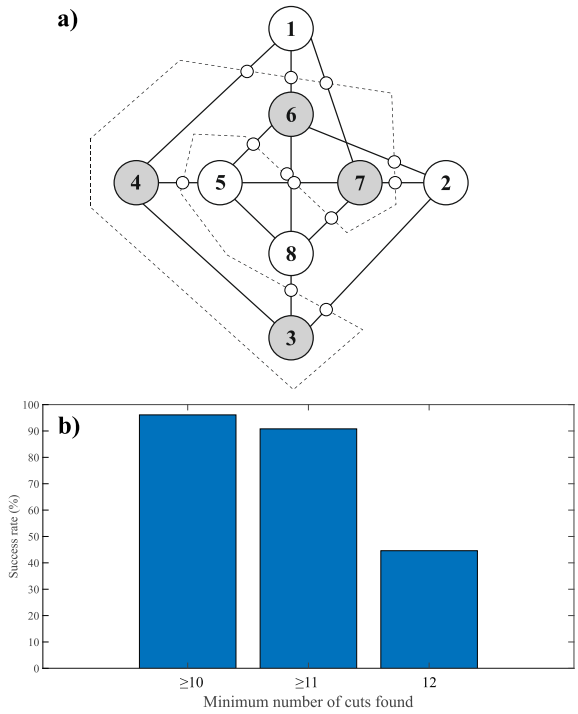

Fig. 15. (a) 8-node Max-Cut problem reported in [10] with 12 cuts (b) Histogram representing the probability of success of obtaining at least 10, 11 or 12 cuts.

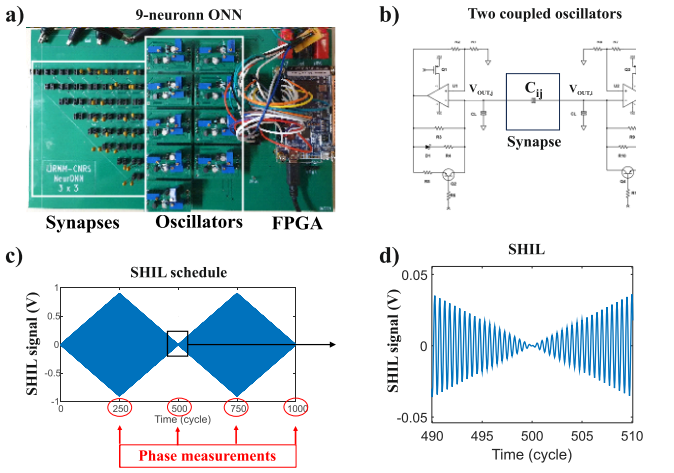

Fig. 16. (a) 9-Neuron ONN on PCB with 36 recurrent synapses. The FPGA initializes and samples the phase at each oscillation cycle and sends the data to a laptop. (b) Schmitt trigger-based relaxation oscillator that emulates a VO2 oscillator. Resistances R3 and R4 set the discharging and charging times, respectively. Q1 is used to turn on the oscillator, while Q2 injects the SHIL signal. (c) Triangular SHIL schedule with a period of 500 cycles. We computed four cuts based on phase measurements at 250, 500, 750, and 1000 cycles. (d) Zoomed view of the SHIL signal around 0V.

because of some reported results using SHIL1. According to [10], the probability of success increases with K_{PER} (their annealing cycles). Thus, an open question is whether this statement holds for SHIL3.

V. Experimental Results

Here, we experimentally investigate the OIM operation protocol using the triangular schedule (SHIL3). There is not a specific controllable source of noise like in simulation, but the one associated to the experimental setup. We designed a 9-node OIM proof-of-concept using off-the-shelf components on a Printed Circuit Board (PCB) shown in Fig 16a. The OIM can implement any 9-node graph with various densities, where graph nodes are oscillators, and edges are synaptic capacitors. Each one of the 9(9−1)/2=36 synapses can be programmed by placing a discrete capacitor in the corresponding support. The oscillator circuit diagram is shown in Fig 16b and consists of a Schmitt trigger-based oscillator that charges and discharges a load capacitance CL, similar to a VO_2 relaxation oscillator. The operating frequency of the OIM is 30kHz. Each oscillator has an SHIL input that receives the sinusoidal synchronization signal at $f = 60$ kHz. An FPGA initializes and samples the phases at each oscillation cycle to enable real-time phase monitoring. The data are sent to a laptop and post-processed with MATLAB.

For each experiment, we map the graph edges to 100 pF-coupling capacitors. For each one of the 100 trials, the oscillators are randomly initialized and driven by the triangular modulation (SHIL3) with two periods of 500 oscillation cycles each (Fig 16c with $K_{PER} = 250$). The cuts are computed based on four sets of phases sampled (read) at K_{PER}, 2· K_{PER}, 3· K_{PER}, and 4· K_{PER} oscillation cycles, and normalized by the Max-Cut value. Note that the sampling times $t = K_{PER}$ and t=3· K_{PER} cycles correspond to the largest SHIL amplitude, while SHIL is OFF when sampling at $t = 2\cdot K_{PER}$ and $t = 4\cdot K_{PER}$ cycles. Thus, comparing the four cuts when SHIL is maximum or minimum gives insight into the cut dynamics. So, we can experimentally validate that decreasing SHIL enables further exploration of the energy landscape.

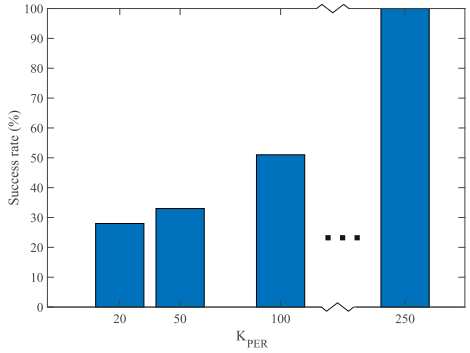

Fig. 17. The success rate for two-cycle SHIL3 with different K_{PER} values.

Fig 17 depicts the success rate for the 6-node in Fig 11 for different K_{PER} values and the procedure described in the previous paragraph. These results are consistent with the success rates obtained in the simulation experiments for T_{COMP1}. T_{COMP1} corresponds to 1.5 SHIL3 cycles, similar to the 2 cycles used here. Note that identical quantitative results are not expected at all.

Fig 18 depicts results also for the 6-node in Fig 11 with $K_{PER} = 250$, but now details of the four readings are shown. The histograms of the normalized cut vales measures when the SHIL amplitude is maximum (first and third histograms) are very different from those obtained with SHIL OFF (second and fourth histograms). Clearly, removing SHIL, the oscillator phases are unfrozen, as we explained before. Thus, allowing

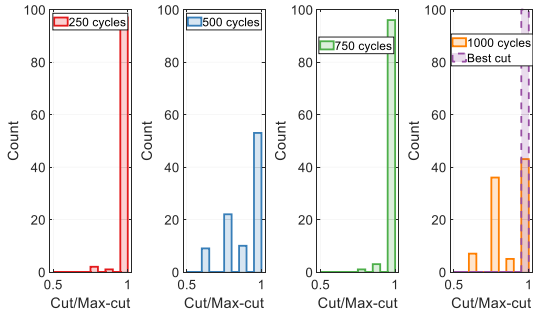

Fig. 18. Histograms of cut values measured at 250, 500, 750, and 1000 oscillation cycles. The purple dashed histogram on the right-hand side shows the best cut among the four values.

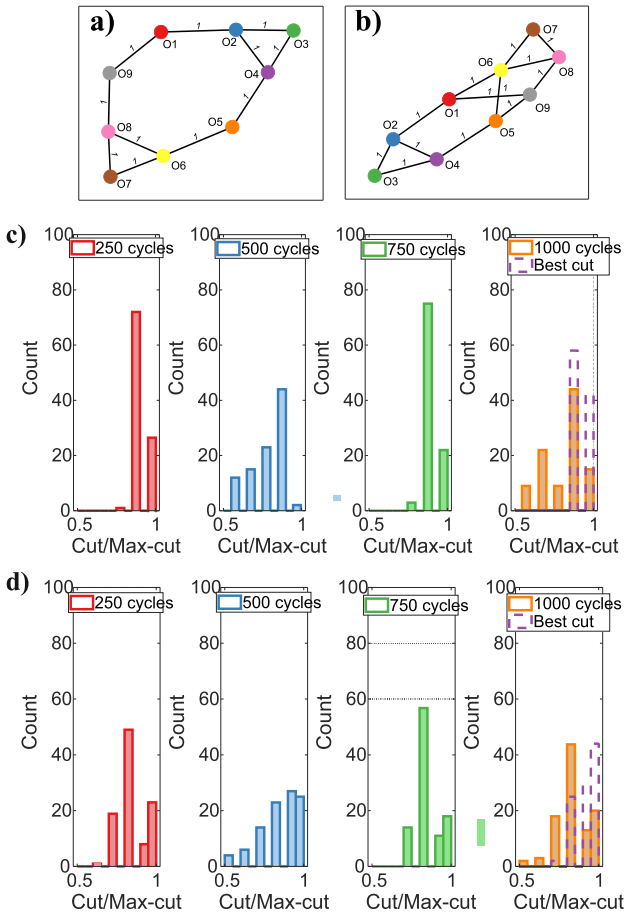

Fig. 19. Histograms of cut values measured at 250, 500, 750, and 1000 cycles (c) for graph (a), (d) for graph (b).

the displacement towards other regions of the energy landscape in which the minimum objective could eventually be found. Note that the number of trials producing the maximum max-cut is similar in readings 1 and 3, however, there are trials for which the first reading exhibits a suboptimal result but an optimum one in the second reading. This is demonstrated by the fact that if the best of all the readings is computed (purple bar in the fourth histogram), the number of attempts that produce a maximum cut is higher than that obtained for each of the readings.

Identical experimental set-up has been applied to two unbalanced 9-node graphs, depicted in Fig 19 together with their histograms. Although improvements associated with the

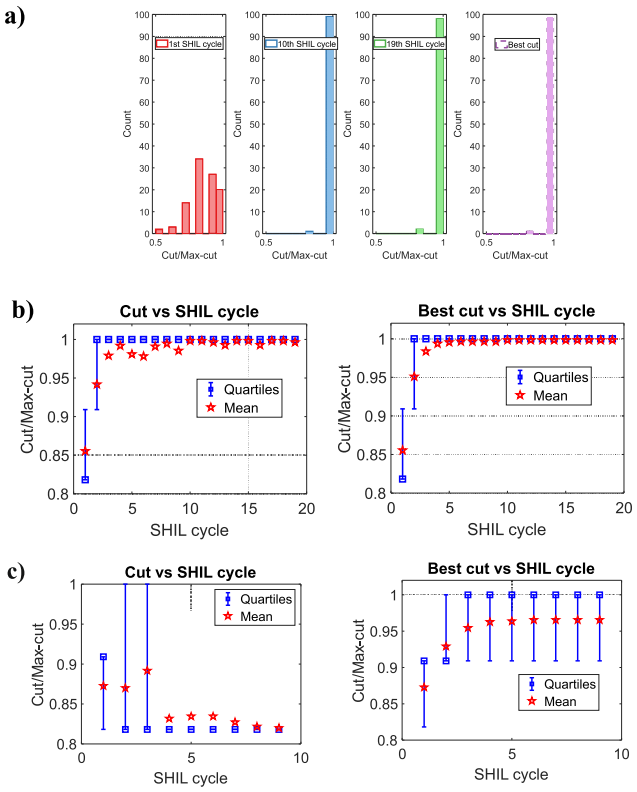

Fig. 20. Results for the graph in Fig 19b, (a) Histograms of cut values measured in the 1st, 10th, and 19th cycles for $K_{PER} = 26$, (b) Cut and best cut versus SHIL cycle for $K_{PER} = 26$, (c) $K_{PER} = 58$.

multi-reading triangular SHIL are observed, the success rate is under 50% for both examples.

Therefore, we investigate alternative SHIL3 configurations assuming a computation time of 1000 oscillation cycles. That is, different values of K_{PER} were used. Lower K_{PER} values allow for more SHIL3 cycles to be accommodated in identical computation time. For a value of $K_{PER} = 250$, as in the previous experiment, two cycles of SHIL3 fit, while for a value of $K_{PER} = 25$ there is room for 20 cycles. Fig 20 shows the results obtained for the graph in Fig 19b. Fig 20a depicts histograms for $K_{PER} = 26$ at the 1st, 10th, and 19th SHIL3 cycles. Fig 20b (c) shows the average cut value over the 100 trials versus the SHIL cycle, as well as the best cut for $K_{PER} = 26$ (58).

It can be observed comparing Fig 19d and Fig 20a that the fraction of trials that reach the ground state or optimal solution to the Max-Cut problem is significantly increased. It is improved from less than 50% to 100%.

It is also interesting to compare Fig 20b and c. The best cut smaller than 1 for $K_{PER} = 58$ (c) indicates that not all the trials led to an optimal solution, in comparison with $K_{PER} = 26$ (b). In the latter case, the evolution of the cut value is more attractive as it increases after each SHIL cycle.

These results indicate that there seems to be an optimal K_{PER} value for which the OIM is driven towards a lower energy state after each SHIL cycle. However, the optimal K_{PER} value is graph-dependent as we had to adjust the K_{PER} value for each graph instance to observe a similar behavior. Overall, a high K_{PER} value corresponds to each SHIL cycle

behaving like a new trial, i.e. the OIM memory is lost during the sequence of SHIL cycles. With K_{PER} <23 the results have worsened, not reaching the 100% success rate, as the SHIL period gets probably smaller than the OIM settling time. This was also observed in VI by sweeping the K_{PER} value.

In summary, results obtained experimentally are in agreement with those found by electrical simulation. In particular, both simulation and experimental results have shown that running long SHIL cycles on our OIM does not necessarily improve the accuracy over time. We believe this is mainly caused by the unlocking of phases when SHIL is OFF which prevents any kind of memory throughout the SHIL operation. However, long SHIL cycles still enable the exploration of a wider region in the energy landscape from a single initial network state. A good compromise seems to occur when both OIM settling and SHIL ramping times are similar. In this regime, the OIM can escape local energy minima that are reached at each SHIL cycle. However, the OIM settling time depends on each input problem and thus the optimal K_{PER} value is not unique. Finally, complementing the proposed SHIL schedule by taking the best cut value among several measurements can increase the success rate, and so the performance of the OIM for solving optimization problems.

VI. Conclusion

This article has shown how a network of coupled oscillators can be operated to solve different computational tasks. It is one of the very few to explore the performance of coupled oscillator networks at the electrical level or by physical implementations. Phase-based simulations used in other works are hardware agnostic and do not consider important effects. Using VO_2 based oscillators, the different operation conditions required to implement an AM or an IM machine with an identical architecture have been illustrated. The IM functionality requires being able to escape from local minimum energy states. Simulation-based analysis of the role of several factors such as SHIL signal, noise, or initial network state in that target behaviour has led to the proposal of a novel SHIL schedule. Its main feature is that the SHIL signal amplitude is increased and decreased. Reducing SHIL strength is the mechanism that enables escape from local minimum energy states. Its combination with a multi-reading scheme can improve the performance of the OIM for solving optimization problems. An experimental OIM has been built to validate our proposal and to further explore the impact of how fast the SHIL amplitude is varied. Our simulation and experimental results solving several instances of Max-Cut optimization problems contribute to a deeper understanding of how to operate a network of coupled oscillators as an Ising machine. Proposed SHIL schedule has shown potential for an efficient exploration of the energy landscape of the associated Ising model for the analyzed OIMs. However, selection of the parameters that configure the SHIL schedule, such as the K_{PER} value or SHIL amplitude, is still an open question that requires further research to analyze graphs with different sparsity and size. Regarding the scalability of our proposal, it is appropriate to point out that this requires abandoning the idea of an all-to-all connection scheme and choosing a specific architecture. The selection of the said architecture and the mapping from the Ising model to the specific architecture is beyond the scope of this paper and is a future line of work.

Acknowledgment

The VO_2 model was provided by IBM-Research, Zurich.

References

[1] F. C. Hoppensteadt and E. M. Izhikevich, "Oscillatory neurocomputers with dynamic connectivity," *Phys. Rev. Lett.*, vol. 82, no. 14, pp. 2983–2986, Apr. 1999, doi: 10.1103/PhysRevLett.82.2983.

[2] A. Raychowdhury et al., "Computing with networks of oscillatory dynamical systems," *Proc. IEEE*, vol. 107, no. 1, pp. 73–89, Jan. 2019, doi: 10.1109/JPROC.2018.2878854.

[3] T. C. Jackson, A. A. Sharma, J. A. Bain, J. A. Weldon, and L. Pileggi, "Oscillatory neural networks based on TMO nano-oscillators and multi-level RRAM cells," *IEEE J. Emerg. Sel. Topics Circuits Syst.*, vol. 5, no. 2, pp. 230–241, Jun. 2015, doi: 10.1109/JETCAS.2015.2433551.

[4] G. Csaba and W. Porod, "Coupled oscillators for computing: A review and perspective," *Appl. Phys. Rev.*, vol. 7, no. 1, Jan. 2020, Art. no. 011302.

[5] Fujitsu. *The White Book of Quantum Computing*. Accessed: 2020. [Online]. Available: https://sp.ts.fujitsu.com/dmsp/Publications/public/Digital_Annealer_White_Book.pdf

[6] A. Lucas, "Ising formulations of many NP problems," *Frontiers Phys.*, vol. 2, Feb. 2014. [Online]. Available: https://www.frontiersin.org/articles/10.3389/fphy.2014.00005/full, doi: 10.3389/fphy.2014.00005.

[7] M. Sao, H. Watanabe, Y. Musha, and A. Utsunomiya, "Application of digital annealer for faster combinatorial optimization," *Fujitsu Sci. Tech. J.*, vol. 55, no. 2, pp. 45–51, 2019.

[8] R. Hamerly et al., "Experimental investigation of performance differences between coherent Ising machines and a quantum annealer," *Sci. Adv.*, vol. 5, no. 5, pp. 1–11, May 2019, doi: 10.1126/sciadv.aau0823.

[9] S. Dutta, A. Khanna, J. Gomez, K. Ni, Z. Toroczkai, and S. Datta, "Experimental demonstration of phase transition nano-oscillator based Ising machine," in *IEDM Tech. Dig.*, San Francisco, CA, USA, Dec. 2019, p. 37.8.1–37.8.4, doi: 10.1109/IEDM19573.2019.8993460.

[10] S. Dutta et al., "An Ising Hamiltonian solver based on coupled stochastic phase-transition nano-oscillators," *Nature Electron.*, vol. 4, no. 7, pp. 502–512, Jul. 2021, doi: 10.1038/s41928-021-00616-7.

[11] J. Núñez et al., "Oscillatory neural networks using VO_2 based phase encoded logic," *Frontiers Neurosci.*, vol. 15, Apr. 2021, Art. no. 655823, doi: 10.3389/fnins.2021.655823.

[12] J. Shamsi, M. J. Avedillo, B. Linares-Barranco, and T. Serrano-Gotarredona, "Effect of device mismatches in differential oscillatory neural networks," *IEEE Trans. Circuits Syst. I, Reg. Papers*, vol. 70, no. 2, pp. 872–883, Feb. 2023, doi: 10.1109/TCSI.2022.3221540.

[13] A. Todri-Sanial et al., "How frequency injection locking can train oscillatory neural networks to compute in phase," *IEEE Trans. Neural Netw. Learn. Syst.*, vol. 33, no. 5, pp. 1996–2009, May 2022, doi: 10.1109/TNNLS.2021.3107771.

[14] C. Delacour and A. Todri-Sanial, "Mapping Hebbian learning rules to coupling resistances for oscillatory neural networks," *Frontiers Neurosci.*, vol. 15, Nov. 2021, Art. no. 694549, doi: 10.3389/fnins.2021.694549.

[15] C. Delacour, S. Carapezzi, M. Abernot, and A. Todri-Sanial, "Energy-performance assessment of oscillatory neural networks based on VO_2 devices for future edge AI computing," *IEEE Trans. Neural Netw. Learn. Syst.*, early access, Jan. 26, 2023, doi: 10.1109/TNNLS.2023.3238473.

[16] S. Carapezzi et al., "Advanced design methods from materials and devices to circuits for brain-inspired oscillatory neural networks for edge computing," *IEEE J. Emerg. Sel. Topics Circuits Syst.*, vol. 11, no. 4, pp. 586–596, Dec. 2021, doi: 10.1109/JETCAS.2021.3128756.

[17] M. K. Bashar, A. Mallick, D. S. Truesdell, B. H. Calhoun, S. Joshi, and N. Shukla, "Experimental demonstration of a reconfigurable coupled oscillator platform to solve the max-cut problem," *IEEE J. Explor. Solid-State Comput. Devices Circuits*, vol. 6, no. 2, pp. 116–121, Dec. 2020, doi: 10.1109/JXCDC.2020.3025994.

[18] P. Maffezzoni, L. Daniel, N. Shukla, S. Datta, and A. Raychowdhury, "Modeling and simulation of vanadium dioxide relaxation oscillators," *IEEE Trans. Circuits Syst. I, Reg. Papers*, vol. 62, no. 9, pp. 2207–2215, Sep. 2015, doi: 10.1109/TCSI.2015.2452332.

[19] E. Corti, B. Gotsmann, K. Moselund, I. Stolichnov, A. Ionescu, and S. Karg, "Resistive coupled VO_2 oscillators for image recognition," in *Proc. IEEE Int. Conf. Rebooting Comput. (ICRC)*, McLean, VA, USA, Nov. 2018, pp. 1–7, doi: 10.1109/ICRC.2018.8638626.

[20] A. Parihar, N. Shukla, S. Datta, and A. Raychowdhury, "Synchronization of pairwise-coupled, identical, relaxation oscillators based on metal-insulator phase transition devices: A model study," *J. Appl. Phys.*, vol. 117, no. 5, Feb. 2015, Art. no. 054902, doi: 10.1063/1.4906783.

[21] J. Wu, L. Jiao, R. Li, and W. Chen, "Clustering dynamics of nonlinear oscillator network: Application to graph coloring problem," *Phys. D, Nonlinear Phenomena*, vol. 240, no. 24, pp. 1972–1978, Dec. 2011, doi: 10.1016/j.physd.2011.09.010.

[22] N. Mohseni, P. L. Mcmahon, and T. Byrnes, "Ising machines as hardware solvers of combinatorial optimization problems," *Nature Rev. Phys.*, vol. 4, no. 6, pp. 363–379, May 2022, doi: 10.1038/s42254-022-00440-8.

[23] S. Matsubara et al., "Digital annealer for high-speed solving of combinatorial optimization problems and its applications," in *Proc. 25th Asia South Pacific Design Autom. Conf. (ASP-DAC)*, Jan. 2020, pp. 667–672, doi: 10.1109/ASP-DAC47756.2020.9045100.

[24] M. Yamaoka, C. Yoshimura, M. Hayashi, T. Okuyama, H. Aoki, and H. Mizuno, "A 20k-spin Ising chip to solve combinatorial optimization problems with CMOS annealing," *IEEE J. Solid-State Circuits*, vol. 51, no. 1, pp. 303–309, Jan. 2016, doi: 10.1109/JSSC.2015.2498601.

[25] H. M. Waidyasooriya and M. Hariyama, "Highly-parallel FPGA accelerator for simulated quantum annealing," *IEEE Trans. Emerg. Topics Comput.*, vol. 9, no. 4, pp. 2019–2029, Oct. 2021, doi: 10.1109/TETC.2019.2957177.

[26] K. Y. Camsari, S. Salahuddin, and S. Datta, "Implementing p-bits with embedded MTJ," *IEEE Electron Device Lett.*, vol. 38, no. 12, pp. 1767–1770, Dec. 2017, doi: 10.1109/LED.2017.2768321.

[27] W. A. Borders, A. Z. Pervaiz, S. Fukami, K. Y. Camsari, H. Ohno, and S. Datta, "Integer factorization using stochastic magnetic tunnel junctions," *Nature*, vol. 573, no. 7774, pp. 390–393, Sep. 2019, doi: 10.1038/s41586-019-1557-9.

[28] T. Inagaki et al., "A coherent Ising machine for 2000-node optimization problems," *Science*, vol. 354, no. 6312, pp. 603–606, Nov. 2016, doi: 10.1126/science.aah4243.

[29] Y. Haribara, S. Utsunomiya, and Y. Yamamoto, "A coherent Ising machine for MAX-CUT problems: Performance evaluation against semidefinite programming and simulated annealing," in *Principles and Methods of Quantum Information Technologies*. Tokyo, Japan: Springer, 2016, pp. 251–262, doi: 10.1007/978-4-431-55756-2_12.

[30] P. L. Mcmahon et al., "A fully programmable 100-spin coherent Ising machine with all-to-all connections," *Science*, vol. 354, no. 6312, pp. 614–617, Nov. 2016, doi: 10.1126/science.aah5178.

[31] T. Wang, L. Wu, P. Nobel, and J. Roychowdhury, "Solving combinatorial optimisation problems using oscillator based Ising machines," *Natural Comput.*, vol. 20, no. 2, pp. 287–306, Jun. 2021, doi: 10.1007/s11047-021-09845-3.

[32] T. Wang, L. Wu, and J. Roychowdhury, "Late breaking results: New computational results and hardware prototypes for oscillator-based Ising machines," 2019, *arXiv:1904.10211*.

[33] T. Wang, L. Wu, and J. Roychowdhury, "New computational results and hardware prototypes for oscillator-based Ising machines," in *Proc. 56th Annu. Design Autom. Conf.*, Las Vegas, NV, USA, Jun. 2019, pp. 2–6, doi: 10.1145/3316781.3322473.

[34] I. Ahmed, P.-W. Chiu, W. Moy, and C. H. Kim, "A probabilistic compute fabric based on coupled ring oscillators for solving combinatorial optimization problems," *IEEE J. Solid-State Circuits*, vol. 56, no. 9, pp. 2870–2880, Sep. 2021, doi: 10.1109/JSSC.2021.3062821.

[35] W. Moy, I. Ahmed, P.-W. Chiu, J. Moy, S. S. Sapatnekar, and C. H. Kim, "A 1,968-node coupled ring oscillator circuit for combinatorial optimization problem solving," *Nature Electron.*, vol. 5, no. 5, pp. 310–317, May 2022, doi: 10.1038/s41928-022-00749-3.

[36] M. Graber and K. Hofmann, "A versatile & adjustable 400 node CMOS oscillator based Ising machine to investigate and optimize the internal computing principle," in *Proc. IEEE 35th Int. System Chip Conf. (SOCC)*, Belfast, U.K., Sep. 2022, pp. 1–6, doi: 10.1109/SOCC56010.2022.9908118.

[37] J. Núñez, S. Thomann, H. Amrouch, and M. J. Avedillo, "Mitigating the impact of variability in NCFET-based coupled-oscillator networks applications," in *Proc. 29th IEEE Int. Conf. Electron., Circuits Syst. (ICECS)*, Glasgow, U.K., Oct. 2022, pp. 1–4, doi: 10.1109/ICECS202256217.2022.9970771.

[38] D. I. Albertsson, M. Zahedinejad, A. Houshang, R. Khymyn, J. Åkerman, and A. Rusu, "Ultrafast Ising machines using spin torque nano-oscillators," *Appl. Phys. Lett.*, vol. 118, no. 11, Mar. 2021, Art. no. 112404, doi: 10.1063/5.0041575.

[39] A. Neogy and J. Roychowdhury, "Analysis and design of sub-harmonically injection locked oscillators," in *Proc. Design, Autom. Test Eur. Conf. Exhib. (DATE)*, Mar. 2012, pp. 1209–1214, doi: 10.1109/DATE.2012.6176677.

[40] M. Jerry, A. Parihar, A. Raychowdhury, and S. Datta, "A random number generator based on insulator-to-metal electronic phase transitions," in *Proc. 75th Annu. Device Res. Conf. (DRC)*, Jun. 2017, pp. 1–2, doi: 10.1109/DRC.2017.7999423.

[41] S. Dutta, A. Khanna, and S. Datta, "Understanding the continuous-time dynamics of phase-transition nano-oscillator-based Ising Hamiltonian solver," *IEEE J. Explor. Solid-State Comput. Devices Circuits*, vol. 6, no. 2, pp. 155–163, Dec. 2020, doi: 10.1109/JXCDC.2020.3045074.

[42] J. Núñez, M. J. Avedillo, and M. Jiménez, "Solving combinatorial optimization problems with coupled phase transition based oscillators," in *Proc. 37th Conf. Design Circuits Integr. Syst. (DCIS)*, Nov. 2022, pp. 1–6.

[43] M. K. Bashar, A. Mallick, and N. Shukla, "Experimental investigation of the dynamics of coupled oscillators as Ising machines," *IEEE Access*, vol. 9, pp. 148184–148190, 2021, doi: 10.1109/ACCESS.2021.3124808.

María J. Avedillo received the Ph.D. degree (summa cum laude) from the Department of Electronics and Electromagnetism, Universidad de Sevilla, in 1992. She joined as an Assistant Professor with Universidad de Sevilla in 1988, where she has been a Full Professor since 2010. In 1989, she was a Researcher with the Department of Analog Design, National Microelectronics Center (currently, Instituto de Microelectrónica de Sevilla). She has authored more than 150 technical papers in leading international journals and conferences. Her current research interests include the design of circuits using emerging devices, including steep slope transistors and phase transition materials, and non-conventional computing paradigms, with an emphasis on energy-constrained applications. In 1994, she received the Kelvin Premium Award from the Council of the Institution of Electrical Engineers for two published articles.

Manuel Jiménez Través (Member, IEEE) received the B.S. degree in electronics, robotics, and mechatronics and the M.S. degree in micro/nanoelectronics from the University of Sevilla, Spain, in 2015 and 2019, respectively. He is currently pursuing the Ph.D. degree in micro/nanoelectronics. He has been a Technical Researcher with the Institute of Microelectronics of Sevilla since 2017 inside the Group of Design and Test of Mixed-Signal Integrated Circuits. His current research interests include emerging devices and circuits, neuro-inspired computing, and oscillator-based computing, especially concerning energy-efficient and low-power circuits.

Corentin Delacour received the Engineering degree from CentraleSupélec, Paris, France, in 2018, and the M.Sc. degree in microelectronics from the Swiss Federal Institute of Technology Lausanne (EPFL), Lausanne, Switzerland, in 2020. He is currently pursuing the Ph.D. degree with the University of Montpellier, Montpellier, France, with a focus on the architecture design for oscillatory neural networks.

Aida Todri-Sanial received the B.S. degree in electrical engineering from Bradley University, IL, USA, in 2001, the M.S. degree in electrical engineering from Long Beach State University, CA, USA, in 2003, and the Ph.D. degree in electrical and computer engineering from the University of California at Santa Barbara in 2009. She was a Visiting Fellow with the Cambridge Graphene Center and the Wolfson College, University of Cambridge, U.K., from 2016 to 2017. Previously, she was a Research and Development Engineer with the Fermi National Accelerator Laboratory, IL, USA. She has also held visiting research positions with Mentor Graphics, Cadence Design Systems, STMicroelectronics, and the IBM Thomas J. Watson Research Center. She is currently a Full Professor with the Electrical Engineering Department, Eindhoven University of Technology, The Netherlands, and the Director of Research for the French National Council of Scientific Research (CNRS). Her current research interests include emerging technologies and novel computing paradigms, such as neuromorphic and quantum computing.

Bernabé Linares-Barranco received the B.S. degree in electronic physics, the M.S. degree in microelectronics, and the Ph.D. degree in high-frequency OTA-C oscillator design from the University of Seville, Spain, in 1986, 1987, and 1990, respectively, and the Ph.D. degree in analog neural network design from Texas A&M University, College Station, TX, USA, in 1991.

From 1988 to 1991, he was a Graduate Student with the Department of Electrical Engineering, Texas A&M University. Since 1991, he has been a Tenured Scientist with Instituto de Microelectrónica de Sevilla, Seville, where he was a Tenured Researcher in 2003 and a Full Professor in 2004. His current research interests include circuit design for telecommunication, VLSI emulators of biological neurons, VLSI neural-based pattern recognition systems, hearing aids, precision circuit design for instrumentation equipment, VLSI transistor mismatch parameters characterization, and neuromorphic spiking circuits and systems.

Juan Núñez received the Telecommunication Engineering degree in 2005 and the Ph.D. degree from the University of Seville, Seville, Spain, in 2011.

Since 2005, he has been with Instituto de Microelectrónica de Sevilla (IMSE-CNM) and the Department of Electronics and Electromagnetism, University of Seville. In 2022, he was a Tenured Scientist with IMSE-CNM. His current research interests include the design of circuits based on unconventional computing paradigms using emerging devices and the development of design strategies for low-power variability-aware and secure circuits based on state-of-the-art CMOS and emerging beyond-CMOS technologies.